Combining a Mass Matrix formulation and a high order dissipation for the discretisation of turbulent flows

A. Belme, H. Ouvrard

INRIA

INSTITUT NATIONAL DE RECHERCHE EN INFORMATIQUE ET EN AUTOMATIQUE

Combining a Mass Matrix formulation and a high order dissipation for the discretisation of turbulent flows

Anca Belme, Hilde Ouvrard

N° 7079

Octobre 2009

Thème NUM

Rapport de recherche

ISSN 0249-6399 ISRN INRIA/RR--7079--FR+ENG

INRIA
SOPHIA ANTIPOLIS

Combining a Mass Matrix formulation and a high order dissipation for the discretisation of turbulent flows

Anca Belme*, Hilde Ouvrard†

Thème NUM — Systèmes numériques
Projet Tropics

Rapport de recherche n° 7079 — Octobre 2009 — 23 pages

Abstract: This study focuses on analysis of a mass matrix scheme with high-order numerical dissipation for the discretisation of three-dimensional turbulent flows.We used a mixed finite element/finite volume formulation for the discretisation of compressible Navier-Stokes equations.VMS-LES turbulence model is performed to simulate the flow around a circular cylinder at a subcritical Reynolds number Re of 3900.

Key-words: numerical schemes, turbulence simulation, compressible

* INRIA, 2004 Route des Lucioles, BP. 93, 06902 Sophia-Antipolis, France
† University of Montpellier II, France

Unité de recherche INRIA Sophia Antipolis
2004, route des Lucioles, BP 93, 06902 Sophia Antipolis Cedex (France)
Téléphone : +33 4 92 38 77 77 — Télécopie : +33 4 92 38 77 65

Combining a Mass Matrix formulation and a high order dissipation for the discretisation of turbulent flows

Résumé : Le présent rapport est focalisé sur l'analyse d'un schéma numérique à matrice de masse et avec une dissipation numérique d'ordre élévé pour la discrétisation des écoulements turbulents tridimensionelles. On a utilisé une formulation mixte éléments/volumes finies pour la discrétisation des équations de Navier-Stokes compressible. Un modèle de turbulence VMS-LES est utilisé pour la simulation d'un écoulement subcritique autour d'un cylindre à nombre de Reynolds Re 3900.

Mots-clés : schémas numériques, simulation de la turbulence, matrice de masse

1 Introduction

A recent approach to LES based on a Variational Multi-Scale (VMS) framework was introduced by Hughes *et al.* in Ref. [4]. The VMS-LES differs fundamentally from the traditional LES in a number of ways. In this approach, one does not filter the Navier-Stokes equations but uses instead a variational projection. This is an important difference because as performed in the traditional LES, filtering works well with periodic boundary conditions but raises mathematical issues in wall-bounded flows. The variational projection avoids these issues. Furthermore, the VMS-LES method *a priori* separates the scales that is, before the simulation is started. And most importantly, it models the effect of the unresolved-scales only in the equations representing the smallest resolved-scales, and not in the equations for the large scales. Consequently, in the VMS-LES, energy is extracted from the fine resolved-scales by a subgrid scale (SGS) eddy-viscosity model, but no energy is directly extracted from the large structures in the flow. The proposed model has been implemented in a numerical solver (AERO) for the Navier-Stokes equations in the case of compressible flows and perfect Newtonian gases, based on a mixed finite-element/finite-volume scheme formulated for unstructured grids made of tetrahedral elements. Finite elements (P1 type) and finite volumes are used to treat the diffusive and convective fluxes, respectively. Concerning the VMS approach, the version proposed in Ref. [5] for compressible flows and for the particular numerical method employed in AERO has been used here. The discretisation of the convective fluxes for the finite volume scheme used in the software AERO exhibits a lack of accuracy in the case of irregular mesh. In order to overcome this problem, we investigate on this work a new mass matrix scheme with high-order numerical dissipation for the discretization of turbulent flows. The present report is organised as follows: we review in Section 2 a mass matrix scheme for the 1D advection equation and we analyse the stability of this scheme for explicit and implicit time advancing using Von Neumann analysis. Section 3 contains the numerical method in 3D case applied to the compressible Navier-Stokes equations, which has been implemented in our CFD software and a short description of the VMS-LES turbulence simulation model. Finally in the last section, one gives some results of the simulation of turbulent flow around a circular cylinder.

2 Mass Matrix Central Differencing scheme for the advection equation

2.1 Spatial 1D MUSCL formulation

Let us first consider the one-dimensional scalar advection model

$$u_t + c(u)_x = 0 \tag{1}$$

2.1.1 Spatial discretisation

The finite-volume method is used for the discretization in space. Let x_j , $1 \leq j \leq N$ denote the discretization points of the mesh. For each discretization point, we state : $u_j \approx u(x_j)$ and we define the control cell C_j as the interval $[x_{j-\frac{1}{2}}, x_{j+\frac{1}{2}}]$ where $x_{j+\frac{1}{2}} = \frac{x_j + x_{j+1}}{2}$.
We define the unknown vector $U = \{u_j\}$ as point approximation values of the function $u(x)$ at each node j of the mesh.

The time advancing scheme is written :

$$U_{j,t} + \Psi_j(U) = 0$$

where the vector $\Psi_j(U)$ is built as follows:

$$\Psi_j(U) = \frac{1}{\Delta x}(\Phi_{j+\frac{1}{2}} - \Phi_{j-\frac{1}{2}});\ \Phi_{j+\frac{1}{2}} = \Phi(u^-_{j+\frac{1}{2}},\, u^+_{j+\frac{1}{2}}); \tag{2}$$

where $u^-_{j\pm\frac{1}{2}}$, $u^+_{j\pm\frac{1}{2}}$ are integration values of u at boundaries of control volume C_j. The Φ's are defined as:

$$\Phi(u,v) = \frac{cu+cv}{2} - \frac{\delta}{2}c(v-u)$$

where δ is a parameter controling the spatial dissipation, such as $\delta \in [0,1]$.
The reconstructed values are then given by: $u^-_{j+\frac{1}{2}} = u_j + \frac{1}{2}\Delta u^-_{j+\frac{1}{2}}$ and $u^+_{j+\frac{1}{2}} = u_j - \frac{1}{2}\Delta u^+_{j+\frac{1}{2}}$ (same reconstruction for $u^-_{j-\frac{1}{2}}$ and $u^+_{j-\frac{1}{2}}$) where the slopes $\Delta u^-_{j+\frac{1}{2}}$ and $\Delta u^+_{j+\frac{1}{2}}$ are defined by:

$$\begin{aligned}\Delta u^-_{j+\frac{1}{2}} = (1-\beta)(u_{j-1}-u_j) + \beta(u_j - u_{j-1})\\ +\theta^c(-u_{j-1}+3u_j-3u_{j+1}+u_{j+2})\\ +\theta^d(-u_{j-2}+3u_{j-1}-3u_j+u_{j+1})\end{aligned}$$

and

$$\begin{aligned}\Delta u^+_{j+\frac{1}{2}} = (1-\beta)(u_{j+1}-u_j) + \beta(u_{j+2} - u_{j+1})\\ +\theta^c(-u_{j-1}+3u_j-3u_{j+1}+u_{j+2})\\ +\theta^d(-u_j+3u_{j+1}-3u_{j+2}+u_{j+3})\end{aligned}$$

It has been shown that choosing $\beta = \frac{1}{3}$, $\theta^c = -\frac{1}{10}$ and $\theta^d = -\frac{1}{15}$, this scheme becomes fifth-order accurate. The numerical dissipation introduced by this scheme is then made of sixth-order derivatives and can be written as:

$$D_j(u) = \frac{D_{j+\frac{1}{2}}(u) - D_{j-\frac{1}{2}}(u)}{\Delta x}$$

where

$$D_{j+\frac{1}{2}}(u) = \frac{\delta c}{60}(-u_{j-2}+5u_{j-1}-10u_j+10u_{j+1}-5u_{j+2}+u_{j+3}) \tag{3}$$

2.2 Mass Matrix Scheme with central differencing

The usual central-differences three-points scheme is penalized by a dispersion leading error, see [1]. This error is compensated introducing the finite-element $P1$ consistent mass matrix. That is, the temporal term of equation (1) is evaluated by Finite Elements. The time advancing is thus written

as:

$$MU(t) + \Delta x \Psi(U) = 0. \tag{4}$$

The finite-element $P1$ mass matrix M is defined as $\big(M\big)_{ij} = \int \Phi^{(i)}\Phi^{(j)}$ where $\Phi^{(i)}$ is the basis function for the finite-element $P1$ formulation. That is: $\Phi^{(i)}$ is a piecewise linear function such as $\Phi^{(i)}(S_i) = 1$ and $\Phi^{(i)}(S_j) = 0$ for all $i \neq j$, where S_j denotes the j-th vertex. M is a three-diagonal matrix equal to:

$$M = \text{Three-diag}(\frac{1}{6}\Delta x, \frac{2}{3}\Delta x, \frac{1}{6}\Delta x)$$

One obtains thus for the j-th component of vector $MU(t)$:

$$(MU(t))_j = m_{j,j-1}U_{j-1,t} + m_{j,j}U_{j,t} + m_{j,j+1}U_{j+1,t}$$

where

$$\begin{aligned} m_{j,j-1} &= 1/6\Delta x \\ m_{j,j} &= 2/3\Delta x \\ m_{j,j+1} &= 1/6\Delta x \ . \end{aligned}$$

Then one can combine this discretisation of the temporal term with a numerical flux for the approximation of the convectif term:

$$\Phi_{j+\frac{1}{2}} = \Phi(u_j, u_{j+1}) = c\big(\frac{u_j + u_{j+1}}{2}\big) - \frac{\delta}{2}T_{j+\frac{1}{2}}$$

Terms $c\big(\frac{u_j + u_{j+1}}{2}\big)$ will contribute to the central differenced flux.
According to the Pascal triangle, a fifth-order difference evaluated between j and $j+1$ can be written as follows ($k > 0$):

$$T_{j+1/2} = kc(-u_{j-2} + 5u_{j-1} - 10u_j + 10u_{j+1} - 5u_{j+2} + u_{j+3})$$

One chooses the constant k as:

$$k = \frac{1}{30} \tag{5}$$

in order to have the same level of dissipation as in the upwind case, see (3).
Finally, starting from expression (2), we get for the operator Ψ_j defined:

$$\begin{aligned} \Psi_j(U) = \frac{c}{2\Delta x}(& \quad k & & u_{j-3} \\ & + \quad (-6k) & & u_{j-2} \\ & + \quad (-1+15k) & & u_{j-1} \\ & + \quad (-20k) & & u_j \\ & + \quad (1+15)k & & u_{j+1} \\ & + \quad (-6k) & & u_{j+2} \\ & \quad k & & u_{j+3}) \end{aligned} \tag{6}$$

2.3 Time advancing stability

2.3.1 Explicit time stepping

Let us consider a time integration of the system $MU_t = AU$, with A the spatial approximation matrix and M the P1 finite element mass matrix. We can combine the above scheme with the linearised six-stage Runge-Kutta scheme:

$$\begin{array}{l} U^{(0)} = U^n \\ U^{(k)} = U^{(0)} + \frac{\Delta t}{N-k+1} M^{-1} \Psi \left(U^{(k-1)} \right), \quad k = 1 \dots N \\ U^{n+1} = U^{(6)} \end{array} \tag{7}$$

The stability study of the scheme is made with the classical Fourier analysis. Let us include in equation (6) the Fourier mode: $\hat{u}_j^n = \overline{u}_k e^{ij\theta_k}$ where θ_k is the frequence parameter.
We obtain:

$$m_\theta \frac{d\hat{u}_j^n}{dt} = -\hat{\Psi}^\delta$$

where $m_\theta = \frac{1}{3}(2 + \cos(\theta))$
$\hat{\Psi}^\delta = \frac{c}{2\Delta x}(R_3 \cos(3\theta) + R_2 \cos(2\theta) + R_1 \cos(\theta) + R_0 + iI_1 \sin(\theta))\hat{u}_j^n$, with:

$$\begin{cases} R_3 = 2\delta k \\ R_2 = -12\delta k \\ R_1 = 30\delta k \\ R_0 = -20\delta k \\ I_1 = 2 \end{cases}$$

denoting λ_θ the linear operator such as $\hat{\Psi}^\delta = -\lambda_\theta \hat{u}_j^n$.
We introduce the Courant number $\nu = \frac{c\Delta t}{\Delta x}$ and the amplification factor $G_\theta = g(z_\theta)$.
$z_\theta = \frac{\lambda_\theta \Delta t}{m_\theta}$, g is the RK6 characteristic polynomial:

$$g(z) = 1 + z + \frac{z^2}{2} + \frac{z^3}{6} + \frac{z^4}{24} + \frac{z^5}{120} + \frac{z^6}{720}$$

Finaly, we have:

$$\begin{cases} z_\theta = -\frac{3\nu}{2(2+\cos(\theta))}(z_\theta^R + iz_\theta^I) \\ z_\theta^R = R_3 \cos(3\theta) + R_2 \cos(2\theta) + R_1 \cos(\theta) + R_0 \\ z_\theta^I = I_1 \sin(\theta) \end{cases}$$

Plotting the gain function $Ga(\nu) = \max_{\theta \in [0,\pi]} g(z_\theta)$, we can determinize ν_{max}, the maximum value of CFL number to obtain a stable scheme with, that is the maximum value of ν such as
$|g(z_\theta)| \leq 1$.
For a CFL small enough, the whole of z_θ complex numbers remains inside the A-Stability region of the RK6 time advancing scheme as illustrated on FIG. (1).

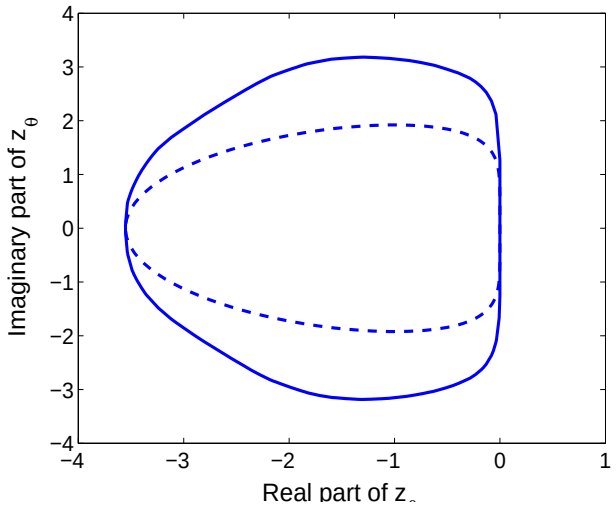

Figure 1: Stability analysis: we depict with the line the boundary of the region for which $g(z) \leq 1$ and (inside) dashed z_θ complex numbers for $\delta = 1$ and $\nu_{max} = 1.11$

2.3.2 Implicit time stepping

The purpose of this section is the stability analysis of the implicit scheme. This can be also done with Fourier analysis. The computation is made on the same one-dimensional scalar conservation law. Let us use the implicit scheme a δ-scheme using a mass-matrix formulation:

$$T^n \delta U^{n+1} = \Delta t^n \Psi(U^n)$$

with $\delta U^{n+1} = U^{n+1} - U^n$ and T^n is the implicit matrix.
In case of a first order scheme, T^n represents the following three-diagonal matrix :

$$T^n = \text{diag}(\tfrac{1}{6} - \nu, \tfrac{2}{3} + \nu, \tfrac{1}{6})$$

With the Fourier analysis we obtain:

$$t_\theta = 1 + \nu(1 - \cos(\theta)) + \tfrac{1}{3}(2 + cos(\theta)) + i\nu \sin(\theta)$$

The amplification factor is then given by:

$$G(\Delta t) = \tfrac{t_\theta + z_\theta}{t_\theta}$$

We are must interested on the behavior of the amplification factor when the time step Δt tends to $+\infty$. The aim is to know if the builds ones schemes are preconditionated at first ordre with satisfactory factors of convergence. Let us denote $\lim_{\Delta t \to \infty} G(\Delta t) = f_\theta(\delta)$. We are searching the Fourier's modes for different schemes witch maximises the functions:

$$f_\theta(\delta) = 1 - \frac{1}{4(1 - \cos(\theta))m_\theta}[(1 - \cos(\theta))z_\theta^R + \sin(\theta)z_\theta^I] + i[\frac{\sin(\theta)z_\theta^R - (1 - \cos(\theta))z_\theta^I}{4m_\theta(1 - \cos(\theta))}]$$

The function f_δ are depicted with three different values of δ in FIG. 2,3 and 4. We can observe that our implicit scheme is inconditionally stable. Let us denote that the optimal value that minimise the gain function when Δt goes to ∞ is $\delta = 1$.

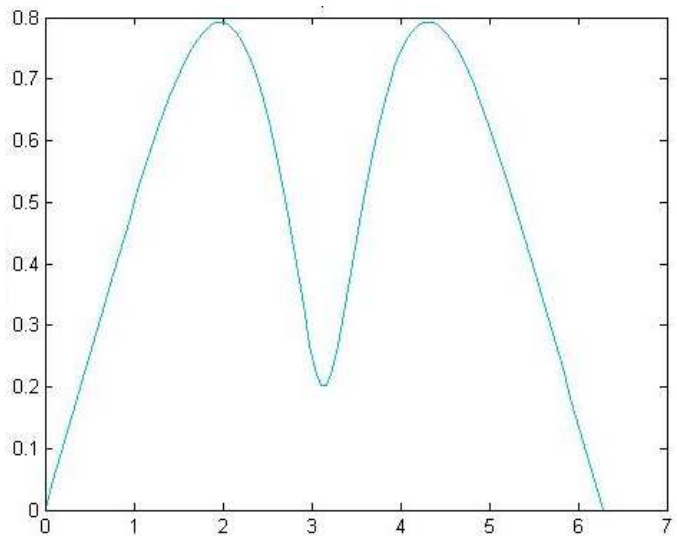

Figure 2: Amplification factor, Δt goes to ∞, case $\delta = 1$

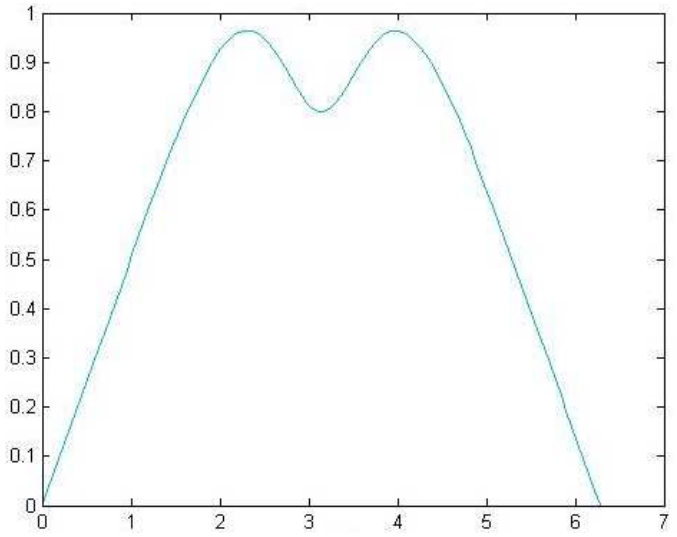

Figure 3: Amplification factor, Δt goes to ∞, case $\delta = 0.5$

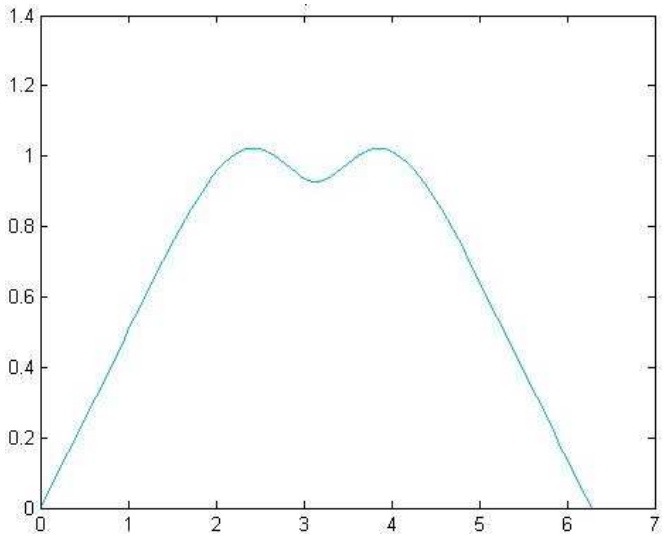

Figure 4: Amplification factor, Δt goes to ∞, case $\delta = 0.3$

3 Numerical Method 3D

3.1 Introduction

In the present chapter the code AERO, used in the present study, is described. The code permits to solve the Euler equations, the Navier-Stokes equations for laminar flows and to use different turbulence models for RANS, LES and hybrid RANS/LES approaches. The unknown quantities are the density, the components of the momentum and the total energy per unit volume. AERO employs a mixed finite-volume/finite-element formulation for the spatial discretization of the equations. Finite-volumes are used for the convective fluxes and finite-elements (P1) for the diffusive ones. The resulting scheme is second order accurate in space. The equations can be advanced in time with explicit low-storage Runge-Kutta schemes. Also implicit time advancing is possible, based on a linearised method that is second order accurate in time.

3.2 Set of equations

In the AERO code the Navier-Stokes equations are numerically normalised with the following reference quantities:

- $L_{ref} \Longrightarrow$ characteristic length of the flow
- $U_{ref} \Longrightarrow$ velocity of the free-stream flow
- $\rho_{ref} \Longrightarrow$ density of the free-stream flow
- $\mu_{ref} \Longrightarrow$ molecular viscosity of the free-stream flow

The flow variables can be normalised with the reference quantities as follows:

$$\rho^* = \frac{\rho}{\rho_{ref}} \qquad u_j^* = \frac{u_j}{U_{ref}} \qquad p^* = \frac{p}{p_{ref}}$$

$$E^* = \frac{E}{\rho_{ref} U_{ref}^2} \qquad \mu^* = \frac{\mu}{\mu_{ref}} \qquad t^* = t\,\frac{L_{ref}}{U_{ref}}\ .$$

The non-dimensional form of the Navier-Stokes equations for the laminar case are reported in the following:

$$\begin{aligned}
\frac{\partial \rho^*}{\partial t^*} + \frac{\partial (\rho^* u_j^*)}{\partial x_j^*} &= 0 \\
\frac{\partial (\rho^* u_i^*)}{\partial t^*} + \frac{\partial \rho^* u_i^* u_j^*}{\partial x_j^*} &= -\frac{\partial p^*}{\partial x_i^*} + \frac{1}{Re}\frac{\partial \sigma_{ij}^*}{\partial x_j^*} \\
\frac{\partial (\rho^* E^*)}{\partial t^*} + \frac{\partial (\rho^* E^* u_j^*)}{\partial x_j^*} &= -\frac{\partial (p^* u_j^*)}{\partial x_j^*} + \frac{1}{Re}\frac{\partial (u_j^* \sigma_{ij}^*)}{\partial x_i^*} - \frac{\gamma}{RePr}\frac{\partial}{\partial x_j^*}\Big[\mu^*\Big(E^* - \frac{1}{2}u_j^* u_j^*\Big)\Big]
\end{aligned} \tag{8}$$

where the Reynolds number, $Re = U_{ref} L_{ref}/\nu$, is based on the references quantities, U_{ref} and L_{ref}, the Prandlt number, Pr, can be assumed constant for a gas and equal to:

$$Pr = \frac{C_p \mu}{k}$$

and $\gamma = C_p/C_v$ is the ratio between the specific heats at constant pressure and volume. Also the constitutive equations for the viscous stresses and the state equations may be written in non-dimensional form as follows:

$$\begin{aligned}
\sigma_{ij}^* &= -\frac{2}{3}\mu^*\Big(\frac{\partial u_k^*}{\partial x_k^*}\delta_{ij}\Big) + \mu^*\Big(\frac{\partial u_i^*}{\partial x_j^*} + \frac{\partial u_j^*}{\partial x_i^*}\Big) \\
p^* &= (\gamma - 1)\rho^*\Big(E^* - \frac{1}{2}u_j^* u_j^*\Big)\ .
\end{aligned} \tag{9}$$

In order to rewrite the governing equations in a compact form more suitable for the discrete formulation, the following unknown variables are grouped together in the $\boldsymbol{W}$ vector:
$\boldsymbol{W} = (\rho,\ \rho u,\ \rho v,\ \rho w,\ \rho E)^T$.
If two other vectors, $\boldsymbol{F}$ and $\boldsymbol{V}$ are defined as function of $\boldsymbol{W}$, as follows:

$$\boldsymbol{F} = \begin{pmatrix} \rho u & \rho v & \rho w \\ \rho u^2 + p & \rho uv & \rho uw \\ \rho uv & \rho v^2 + p & \rho vw \\ \rho uw & \rho vw & \rho w^2 + p \end{pmatrix}$$

and

$$\boldsymbol{V} = \begin{pmatrix} 0 & 0 & 0 \\ \sigma_{xx} & \sigma_{yx} & \sigma_{zx} \\ \sigma_{xy} & \sigma_{yy} & \sigma_{zy} \\ \sigma_{xz} & \sigma_{yz} & \sigma_{zz} \\ u\sigma_{xx} + v\sigma_{xy} + w\sigma_{xz} - q_x & u\sigma_{xy} + v\sigma_{yy} + w\sigma_{yz} - q_y & u\sigma_{xz} + v\sigma_{yz} + w\sigma_{zz} - q_z \end{pmatrix}$$

they may be substituted in (8), to get a different compact format of the governing equations which is the starting point for the derivation of the Galerkin formulation and of the discretization of the problem:

$$\frac{\partial \boldsymbol{W}}{\partial t} + \frac{\partial}{\partial x_j} F_j(\boldsymbol{W}) - \frac{1}{Re}\frac{\partial}{\partial x_j} V_j(\boldsymbol{W}, \nabla \boldsymbol{W}) = 0 \ . \tag{10}$$

It is important to stress that the vectors $\boldsymbol{F}$ and $\boldsymbol{V}$ are respectively the convective fluxes and the diffusive fluxes.

3.3 Spatial discretization

Spatial discretization is based on a mixed finite-volume/finite-element formulation. A finite volume upwind formulation is used for the treatment of the convective fluxes while a classical Galerkin finite-element centred approximation is employed for the diffusive terms .
The computational domain Ω is approximated by a polygonal domain Ω_h. This polygonal domain is then divided in N_t tetrahedrical elements T_i by a standard finite-element triangulation process:

$$\Omega_h = \bigcup_{i=1}^{N_t} T_i. \tag{11}$$

The set of elements T_i forms the grid used in the finite-element formulation. The dual finite-volume grid can be built starting from the triangulation following the medians method.
In the medians method a finite-volume cell is constructed around each node a_i of the triangulation, dividing in 4 sub-tetrahedra every tetrahedron having a_i as a vertex by means of the median planes. C_i is the union of the resulting sub-tetrahedra having a_i as a vertex and they have the following property:

$$\Omega_h = \bigcup_{i=1}^{N_c} C_i. \tag{12}$$

where N_c is the number of cells, which is equal to the number of the nodes of the triangulation.

3.3.1 Convective fluxes

Indicating the basis functions for the finite-volume formulation as follows:

$$\psi^{(i)}(P) = \begin{cases} 1 & \text{if } P \in C_i \\ 0 & \text{otherwise} \end{cases}$$

the Galerkin formulation for the convective fluxes is obtained by multiplying the convective terms of (10) by the basis function $\psi^{(i)}$, integrating on the domain Ω_h and using the divergence theorem. In this way the results are:

$$\iint_{\Omega_h} \Big(\frac{\partial F_j}{\partial x_j}\Big)\psi^{(i)}\, x\, y = \iint_{C_i} \frac{\partial F_j}{\partial x_j}\, \Omega = \int_{\partial C_i} F_j n_j\, \sigma$$

where $d\Omega$, $d\sigma$ and n_j are the elementary measure of the cell, of its boundary and the jth component of the normal external to the cell C_i respectively.
The total contribution to the convective fluxes is:

$$\sum_j \int_{\partial C_{ij}} \mathcal{F}(\boldsymbol{W}, \vec{n})\, \sigma$$

where j are all the neighbouring nodes of i, $\mathcal{F}(\boldsymbol{W}, \vec{n}) = F_j(\boldsymbol{W}) n_j$, ∂C_{ij} is the boundary between cells C_i and C_j, and $\vec{n}$ is the outer normal to the cell C_i.

The basic component for the approximation of the convective fluxes is the Roe scheme, Ref. [15]:

$$\int_{\partial C_{ij}} \mathcal{F}(\boldsymbol{W}, \vec{n})\, \sigma \simeq \Phi^R(W_i, W_j, \vec{\nu}_{ij})$$

where

$$\vec{\nu}_{ij} = \int_{\partial C_{ij}} \vec{n}\, \sigma$$

and W_k is the solution vector at the k-th node of the discretization.
In the V6 scheme developped in [7] and [6]. The numerical fluxes, Φ^R, are evaluated as follows:

$$\Phi^R(W_i, W_j, \vec{\nu}_{ij}) = \underbrace{\frac{\mathcal{F}(W_i, \vec{\nu}_{ij}) + \mathcal{F}(W_j, \vec{\nu}_{ij})}{2}}_{centred} - \underbrace{\gamma_s\, d^R(W_i, W_j, \vec{\nu}_{ij})}_{upwinding}$$

where $\gamma_s \in [0, 1]$ is a parameter which directly controls the upwinding of the scheme and

$$d^R(W_i, W_j, \vec{\nu}_{ij}) = \left| \mathcal{R}(W_i, W_j, \vec{\nu}_{ij}) \right| \frac{W_j - W_i}{2} \ . \tag{13}$$

$\mathcal{R}$ is the Roe matrix and is defined as:

$$\mathcal{R}(W_i, W_j, \vec{\nu}_{ij}) = \frac{\partial \mathcal{F}}{\partial \boldsymbol{W}}(\widehat{\boldsymbol{W}}, \nu_{ij}) \tag{14}$$

where $\widehat{\boldsymbol{W}}$ is the Roe average between W_i and W_j.
The classical Roe scheme is obtained as a particular case by imposing $\gamma_s = 1$. The accuracy of this scheme is only $1st$ order. In order to increase the order of accuracy of the scheme the MUSCL (*Monotone Upwind Schemes for Conservation Laws*) reconstruction method, introduced by Van Leer, Ref. [19], is employed. This method expresses the Roe flux as a function of W_{ij} and W_{ji}, the extrapolated values of $\boldsymbol{W}$ at the interface between two cells C_i and C_j:

$$\int_{\partial C_{ij}} \mathcal{F}(\boldsymbol{W}, \vec{n})\, \sigma \simeq \Phi^R(W_{ij}, W_{ji}, \vec{\nu}_{ij})$$

where W_{ij} and W_{ji} are defined as follows:

$$W_{ij} = W_i + \frac{1}{2}(\vec{\nabla}\boldsymbol{W})_{ij} \cdot \vec{ij} \ ,$$
$$W_{ji} = W_j + \frac{1}{2}(\vec{\nabla}\boldsymbol{W})_{ji} \cdot \vec{ij} \ .$$

To estimate the gradients $(\vec{\nabla}\boldsymbol{W})_{ij} \cdot \vec{ij}$ and $(\vec{\nabla}\boldsymbol{W})_{ji} \cdot \vec{ij}$, one used these expressions, Ref. [6]:

$$
\begin{aligned}
(\vec{\nabla}\boldsymbol{W})_{ij}\cdot\vec{ij} &= (1-\beta)(\vec{\nabla}\boldsymbol{W})^C_{ij}\cdot\vec{ij}) + \beta(\vec{\nabla}\boldsymbol{W})^U_{ij}\cdot\vec{ij}) + \\
&\quad \xi_c\left[(\vec{\nabla}\boldsymbol{W})^U_{ij}\cdot\vec{ij}) - 2(\vec{\nabla}\boldsymbol{W})^C_{ij}\cdot\vec{ij}) + (\vec{\nabla}\boldsymbol{W})^D_{ij}\cdot\vec{ij})\right] + \\
&\quad \xi_d\left[(\vec{\nabla}W)_M\cdot\vec{ij}) - 2(\vec{\nabla}W)_i\cdot\vec{ij}) + (\vec{\nabla}W)^D_j\cdot\vec{ij})\right] ,
\end{aligned}
$$

$$
\begin{aligned}
(\vec{\nabla}\boldsymbol{W})_{ji}\cdot\vec{ji} &= (1-\beta)(\vec{\nabla}\boldsymbol{W})^C_{ji}\cdot\vec{ij}) + \beta(\vec{\nabla}\boldsymbol{W})^U_{ji}\cdot\vec{ij}) + \\
&\quad \xi_c\left[(\vec{\nabla}\boldsymbol{W})^U_{ji}\cdot\vec{ij}) - 2(\vec{\nabla}\boldsymbol{W})^C_{ji}\cdot\vec{ij}) + (\vec{\nabla}\boldsymbol{W})^D_{ji}\cdot\vec{ij})\right] + \\
&\quad \xi_d\left[(\vec{\nabla}\boldsymbol{W})_{M'}\cdot\vec{ij}) - 2(\vec{\nabla}\boldsymbol{W})_i\cdot\vec{ij}) + (\vec{\nabla}\boldsymbol{W})^D_j\cdot\vec{ij})\right] ,
\end{aligned}
$$

where $(\vec{\nabla}\boldsymbol{W})_i$ and $(\vec{\nabla}\boldsymbol{W})_j$ are the nodal gradients at the nodes i and j respectively and are calculated as the average of the gradient on the tetrahedra $T \in C_i$, having the node i as a vertex. For example for $(\vec{\nabla}\boldsymbol{W})_i$ we can write:

$$
(\vec{\nabla}\boldsymbol{W})_i = \frac{1}{Vol(C_i)}\sum_{T\in C_i}\frac{Vol(T)}{3}\sum_{k\in T} W_k\vec{\nabla}\Phi^{(i,T)} \ . \tag{15}
$$

where $\Phi^{(i,T)}$ is the P1 finite-element basis function. In the 3D case, these functions are so defined:

$$
\Phi^{(i)}(P) = \begin{cases} 1 & \text{if } P = S_i \\ 0 & \text{if } P = S_j, \ \ i \neq j \end{cases}
$$

$(\vec{\nabla}\boldsymbol{W})_M\cdot\vec{ij}$, for the 3D case, is the gradient at the point M in Fig. 5 and it is computed by interpolation of the nodal gradient values at the nodes contained in the face opposite to the upwind tetrahedron T_{ij}. $(\vec{\nabla}\boldsymbol{W})_{M'}\cdot\vec{ij}$ is the gradient at the point M' in Fig. 5 and it is evaluated in the same way as $(\vec{\nabla}\boldsymbol{W})_M\cdot\vec{ij}$. The coefficients β, ξ_c, ξ_d are parameters that control the combination of fully upwind and centred slopes. The V6 scheme is obtained by choosing them to have the best accuracy on cartesian meshes, Ref.[7]:

$$
\beta = 1/3, \qquad \xi_c = -1/30, \qquad \xi_d = -2/15 \ .
$$

The variant of the above scheme called mass-matrix with central differencing, sets β, ξ_c and ξ_d to zero and involves a time derivative evaluated with the finite-element consistent mass matrix. This mass matrix as in the 1D case is expressed in terms of the usual P1 test functions as follows:

$$
M_{ij} = \int \phi^{(i)}\phi^{(j)} d\nu
$$

As in Section 2, we can combine this time derivative with a flux. We get thus the following semi-discretization equation:

$$
\frac{\partial \boldsymbol{W_i}}{\partial t} = \Delta t M^{-1}\sum_j \Phi(\boldsymbol{W_i}, \boldsymbol{W_j}, \vec{\nu_{ij}})
$$

with the numerical flux defined by:

$$
\Phi(W_i, W_j, \vec{\nu_{ij}}) = \frac{\mathcal{F}(W_i, \vec{\nu_{ij}}) + \mathcal{F}(W_j, \vec{\nu_{ij}})}{2} - \frac{\gamma_s}{2}\left|\mathcal{R}(W_i, W_j, \vec{\nu_{ij}})\right|\Delta W_{ij}
$$

where:

$$\Delta W_{ij} = C(2(\vec{\nabla}W)_M.\vec{ij} - 5(\vec{\nabla}W)^u_{ij}.\vec{ij} + 6(\vec{\nabla}W)^c_{ij}.\vec{ij} - 5(\vec{\nabla}W)^d_{ij}.\vec{ij} + 2(\vec{\nabla}W)_{M'}.\vec{ij}) \ .$$

Following the study done for the 1D advection equation (see equation 5), the constant C is set to:

$$C = \frac{\delta}{60} \tag{16}$$

A variant of this scheme is also investigated and consists in using a projected dissipation in $\vec{ij}$: $|\mathcal{R}(W_i, W_j, \nu_{\vec{ij}})|$ becomes $\left|\mathcal{R}(W_i, W_j, \tilde{\nu_{\vec{ij}}})\right|$ in which $\tilde{\nu_{\vec{ij}}} = (\nu_{\vec{ij}}.\frac{\vec{ij}}{\|\vec{ij}\|})\frac{\vec{ij}}{\|\vec{ij}\|}$ This option has been

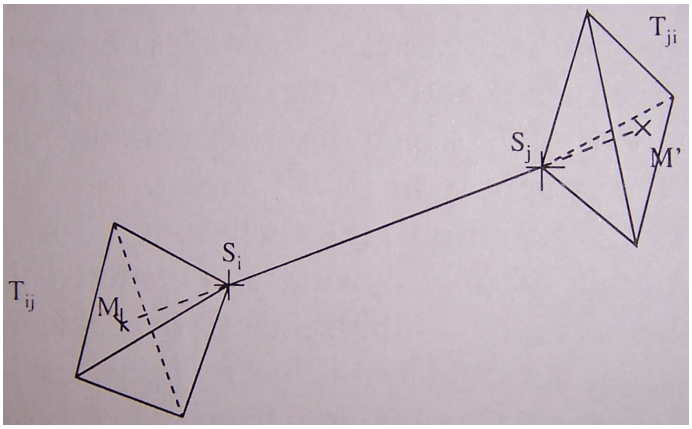

Figure 5: Sketch of points and elements involved in the computation of gradient

investigated for the application of a Gaussian function translation in section 5.1

3.3.2 Diffusive fluxes

The P1 finite-element basis function, $\phi^{(i,T)}$, restricted to the tetrahedron T is assumed to be of unit value on the node i and to vanish linearly at the remaining vertexes of T. The Galerkin formulation for the diffusive terms is obtained by multiplying the diffusive terms by $\phi^{(i,T)}$ and integrating over the domain Ω_h:

$$\iiint_{\Omega_h} \Big(\frac{\partial V_j}{\partial x_j}\Big)\phi^{(i,T)}\,\Omega = \iiint_T \frac{\partial V_j}{\partial x_j}\phi^{(i,T)}\,\Omega \ . \tag{17}$$

Integrating by parts the right-hand side of equation (17) we obtain:

$$\iiint_T \frac{\partial V_j}{\partial x_j}\phi^{(i,T)}\,\Omega = \iiint_T \frac{\partial (V_j\phi^{(i,T)})}{\partial x_j}\,\Omega - \iiint_T V_j\frac{\partial \phi^{(i,T)}}{\partial x_j}\,\Omega = \iint_{\partial T} V_j\phi^{(i,T)}n_j\,\sigma - \iiint_T V_j\frac{\partial \phi^{(i,T)}}{\partial x_j}\,\Omega \ . \tag{18}$$

In order to build the fluxes for the node i consistently with the finite-volume formulation, the contribution of all the elements having i as a vertex needs to be summed together as follows:

$$\sum_{T,i\,\in\,T}\Big(\int_{\partial T} V_j\phi^{(i,T)}n_j\,\sigma - \iint_T V_j\frac{\partial\phi^{(i,T)}}{\partial x_j}\,\Omega\Big) =$$
$$-\sum_{T,i\,\in\,T}\iint_T V_j\frac{\partial\phi^{(i,T)}}{\partial x_j}\,\Omega + \int_{\Gamma_h=\partial\Omega_h}\phi^{(i,T)}V_j n_j\,\sigma\ . \tag{19}$$

In the P1 formulation for the finite-element method, the test functions, $\phi^{(i,T)}$, are linear functions on the element T and so their gradient is constant. Moreover, in the variational formulation the unknown variables contained in $\boldsymbol{W}$ are also approximated by their projection on the P1 basis function. For these reasons the integral can be evaluated directly.

3.4 Boundary conditions

Firstly, the real boundary Γ is approximated by a polygonal boundary Γ_h that can be split in two parts:

$$\Gamma_h = \Gamma_\infty + \Gamma_b \tag{20}$$

where the term Γ_∞ represents the far-fields boundary and Γ_b represents the body surface. The boundary conditions are set using the Steger-Warming formulation ([18]) on Γ_∞ and using slip or no-slip conditions on Γ_b.

3.5 Time advancing

Once the equations have been discretized in space, the unknown of the problem is the solution vector at each node of the discretization as a function of time, $\boldsymbol{W}_h(t)$. Consequently the spatial discretization leads to a set of ordinary differential equations in time:

$$\frac{d\boldsymbol{W}_h}{dt} + \Psi(\boldsymbol{W}_h) = 0 \tag{21}$$

where Ψ_i is the total flux, containing both convective and diffusive terms, of W_h through the i-th cell boundary divided by the volume of the cell.

3.5.1 Explicit time advancing

In the explicit case a N-step low-stockage Runge-Kutta algorithm is used for the discretization of Eq.(21):

$$\begin{cases} \boldsymbol{W}^{(0)} = \boldsymbol{W}^{(n)}, \\ \boldsymbol{W}^{(k)} = \boldsymbol{W}^{(0)} + \Delta t\ \alpha_k\ \Psi(\boldsymbol{W}^{(k-1)}), \quad k = 1, \dots, N \\ \boldsymbol{W}^{(n+1)} = \boldsymbol{W}^{(N)}. \end{cases}$$

in which the suffix h has been omitted for sake of simplicity. Different schemes can be obtained varying the number of steps, N, and the coefficients α_k.

3.5.2 Implicit time advancing

For the implicit time advancing scheme in AERO the following second order accurate backward difference scheme is used:

$$\alpha_{n+1}\boldsymbol{W}^{(n+1)} + \alpha_n \boldsymbol{W}^{(n)} + \alpha_{(n-1)}\boldsymbol{W}^{(n-1)} + \Delta t^{(n)}\Psi(\boldsymbol{W}^{(n+1)}) = 0 \tag{22}$$

where the coefficients α_n can be expressed as follows:

$$\alpha_{n+1} = \frac{1+2\tau}{1+\tau}, \qquad \alpha_n = -1-\tau, \qquad \alpha_{n-1} = \frac{\tau^2}{1+\tau} \tag{23}$$

where $\Delta t^{(n)}$ is the time step used at the n-th time iteration and

$$\tau = \frac{\Delta t^{(n)}}{\Delta t^{(n-1)}}. \tag{24}$$

The nonlinear system obtained can be linearised as follows:

$$\begin{aligned}\alpha_{n+1}\boldsymbol{W}^{(n)} + \alpha_n \boldsymbol{W}^{(n)} + \alpha_{(n-1)}\boldsymbol{W}^{(n-1)} + \Delta t^{(n)}\Psi(\boldsymbol{W}^{(n)}) = \\ - \left[\alpha_{n+1} + \delta t^{(n)}\frac{\partial \Psi}{\partial \boldsymbol{W}}(\boldsymbol{W}^{(n)})\right](\boldsymbol{W}^{(n+1)} - \boldsymbol{W}^{(n)}).\end{aligned} \tag{25}$$

Following the defect-correction approach, the jacobians are evaluated using the 1st order flux scheme (for the convective part), while the explicit fluxes are composed with 2nd order accuracy. The resulting linear system is solved by a Schwarz method.

4 Variational Multiscale approach for Large Eddy Simulation

A new approach to LES based on a variational multiscale(VMS)framework was recently introduced in Hughes *et al.* The VMS-LES differs fundamentally from the traditional LES in a number of ways. In this new approach, one does not filter the Navier-Stokes equations but uses instead a variational projection. This is an important difference because as performed in the traditional LES, filtering works as well with periodic boundary conditions but raises mathematical issues in wall-bounded flows. The variational projection avoids this issues. Furthermore, the VMS-LES method *a priori* separates the scales that is, before the simulation is started. And most importantly, it models the effect of the unresolved-scales only in the equations representing the smallest resolved-scales, and not in the equations for the large scales. Consequently, in the VMS-LES, energy is extracted from the fine resolved-scales by a traditional model such as Smagorinsky eddy viscosity model, but no energy is directly extracted from the large structures in te flow. For this reason, one can reasonably hope to obtain a better behavior near walls, and less dissipation in the presence of large coherent structures.

A less fundamental, yet noteworthy, difference between the VMS-LES and traditional LES methods is that the VMS-LES approach leads to governing equations that are written in terms of the original (or undecomposed) flow variables and the modeled effect of the unresolved-scales on the

smallest resolved one, whereas the classical LES formulation leads to governing equations that are written in terms of the filtered flow variables and modeled subgrid-scales. Hence, in the traditional LES formulation, one first filters the Navier-Stokes equations, then decomposes the flow variables into their filtered and fluctuating parts in the subgrid-tensor, then faces the issues of modeling the subgrid-scales. In the VMS-LES approach, one does not have to decompose into space-averaged and fluctuating parts each occurence in the Navier-Stokes equations of each flow variable because the final equations are expected to be expressed in terms of the importance as it can be exploited to bypass the modeling of some fluctuating quantities, as will be illustrated here for compressible turbulent flows.

The initial developement of the VMS-LES method focused on incompressible turbulent flows, regular grids, and spectral discretisations where the separaton a priori of the scales is simple to achieve. For finite element approximations, a hierarchical basis approach and an alternative method based on cell agglomeration were recently proposed for separating a priori the coarse- and fine-scales. In most cases, the VMS-LES method was applied mainly to homogeneous isotropic incompressible turbulence, and recently to incompressible turbulent channel flows, fo witch it demonstrated an improvement over the traditional LES method.

In this Variational Multiscale approach for Large Eddy Simulation (VMS-LES) approach the flow variables are decomposed as follows:

$$w_i = \underbrace{\overline{w}_i}_{LRS} + \underbrace{w_i'}_{SRS} + {w_i}^{SGS} \tag{26}$$

where $\overline{w}_i$ are the large resolved scales (LRS), w_i' are the small resolved scales (SRS) and ${w_i}^{SGS}$ are the unresolved scales. This decomposition is obtained by variational projection in the LRS and SRS spaces respectively. In the present study, we follow the VMS approach proposed in Ref.[5] for the simulation of compressible turbulent flows through a finite volume/finite element discretization on unstructured tetrahedral grids. If ψ_l are the N finite-volume basis functions and ϕ_l the N finite-element basis fonctions associated to the used grid,in order to obtain the VMS flow decomposition in Eq. (26), the finite dimensional spaces $\mathcal{V}_{FV}$ and $\mathcal{V}_{FE}$, respectively spanned by ψ_l and ϕ_l, can be in turn decomposed as follows [5]:

$$\mathcal{V}_{FV} = \overline{\mathcal{V}}_{FV} \bigoplus \mathcal{V}'_{FV} \; ; \quad \mathcal{V}_{FE} = \overline{\mathcal{V}}_{FE} \bigoplus \mathcal{V}'_{FE} \tag{27}$$

in which $\bigoplus$ denotes the direct sum and $\overline{\mathcal{V}}_{FV}$ and $\mathcal{V}'_{FV}$ are the finite volume spaces associated to the largest and smallest resolved scales, spanned by the basis functions $\overline{\psi_l}$ and ψ_l'; $\overline{\mathcal{V}}_{FE}$ and $\mathcal{V}'_{FE}$ are the finite element analogous. In Ref.[5] a projector operator P in the LRS space is defined by spatial average on macro cells in the following way:

$$\overline{\boldsymbol{W}} = P(\boldsymbol{W}) = \sum_k \underbrace{\left(\frac{Vol(C_k)}{\sum_{j \epsilon I_k} Vol(C_j)} \sum_{j \epsilon I_k} \psi_j \right)}_{\overline{\psi}_k} \boldsymbol{W}_k \tag{28}$$

for the convective terms, discretized by finite volumes, and:

$$\overline{\boldsymbol{W}} = P(\boldsymbol{W}) = \sum_k \underbrace{\left(\frac{Vol(C_k)}{\sum_{j \epsilon I_k} Vol(C_j)} \sum_{j \epsilon I_k} \phi_j \right)}_{\overline{\phi}_k} \boldsymbol{W}_k \tag{29}$$

for the diffusive terms, discretized by finite elements. In both Eqs. (28) and (29),
$I_k = \{j / C_j \in C_{m(k)}\}$, $C_{m(k)}$ being the macro-cell containing the cell C_k. The macro-cells are obtained by a process known as agglomeration [9]. The basis functions for the SRS space are clearly obtained as follows: $\psi_l' = \psi_l - \overline{\psi}_l$ and $\phi_l' = \phi_l - \overline{\phi}_l$.
A key feature of the VMS-les approach is that the modeled influence of the unresolved scales on large resolved ones is set to zero, and so the SGS model is added only to the smallest resolved scales (which models the dissipative effect of the unresolved scales on small resolved ones). This leads to the following equations after semi-discretizations [5].

$$\begin{aligned}
\int_{C_i} \frac{\partial \rho}{\partial t} \Omega + \int_{\partial C_i} \rho \vec{V}.\vec{n} \Gamma &= 0 \\
\int_{C_i} \frac{\partial \rho \vec{V}}{\partial t} \Omega + \int_{\partial C_i} \rho \vec{V} \otimes \vec{V} \vec{n} \Gamma + \int_{\partial C_i} p \vec{n} \Gamma & \\
+ \frac{1}{Re} \int_\Omega \sigma \nabla \Phi_i \Omega + \frac{1}{Re} \int_\Omega \tau^{'} \nabla \Phi_i^{'} \Omega &= 0 \\
\int_{C_i} \frac{\partial E}{\partial t} \Omega + \int_{\partial C_i} (E+p) \vec{V}.\vec{n} \Gamma + \int_\Omega \sigma \vec{V}.\nabla \Phi_i \Omega & \\
+ \frac{\gamma}{RePr} \int_\Omega \nabla e.\nabla \Phi_i \Omega + \frac{\gamma}{RePr_t} \int_\Omega \mu_t^{'} \nabla e^{'}.\nabla \Phi_i^{'} \Omega &= 0
\end{aligned} \tag{30}$$

where e denotes the internal energy ($E = e + \frac{1}{2}\vec{V}^2$) with $\vec{V} = (u_1, u_2, u_3)$ the velocity. $\tau^{'}$ is the small resolved scales SGS stress giben by:

$$\tau^{'} = \mu_t^{'}(2S_{ij}^{'} - \frac{2}{3} S_{kk}^{'} \delta_{ij})$$

with $S_{ij}^{'} = \frac{1}{2}(\frac{\partial u_i^{'}}{\partial x_j} + \frac{\partial u_j^{'}}{\partial x_i})$ and $\mu_t^{'}$, the small resolved scales eddy viscosity (which depends on the chosen SGS model).

One can notice that the laminar Navier-Stokes equations are recovered by substituting $\tau^{'} = 0$ and $\mu_t^{'} = 0$ in Eq. (30) above an that the SGS model is recovered by substituting $\tau^{'} = \tau$, $\mu_t^{'} = \mu_t$, $e^{'} = e$ and $\Phi_i^{'} = \Phi_i$ in the equations, where τ and μ_t denote the usual SGS stress tensor and SGS eddy viscosity, respectively.

More details about this VMS-LES methodology can be found in Ref. [5] and [2].

5 Applications

5.1 Gaussian translation in an irregular mesh

The graph of a gaussian is a characteristic symmetric " bell shape curve " that quickly falls towards plus/minus infinity.
For our 2D study, we consider the advection equation:

$$\frac{\partial \rho}{\partial t}(x,y,t) + c\frac{\partial \rho}{\partial x_i}(x,y,t) = 0$$

using an advection vector $c = (0,1)$ and a gaussian function as initial condition:

$$\rho(x,y,z,0) = 1 + \exp^{-150(x+0,3)}$$

The advection equation is solved using the Mass Lumping V6 scheme and the Mass Matrix Central Differencing scheme with two options: projected dissipation and non projected dissipation as described in section 3.3. Recalling that a "Mass lumping" scheme means that the temporal term of the equations is treated by Finite Volume whereas Mass-Matrix scheme means a temporal term treated by Finite Element. We are in particular interested on the dissipation of the gaussian when it is translated using different meshes. The first mesh is regular as shown FIG. 6 and the second one is irregular with strong variations of the local mesh size (see FIG. 9)

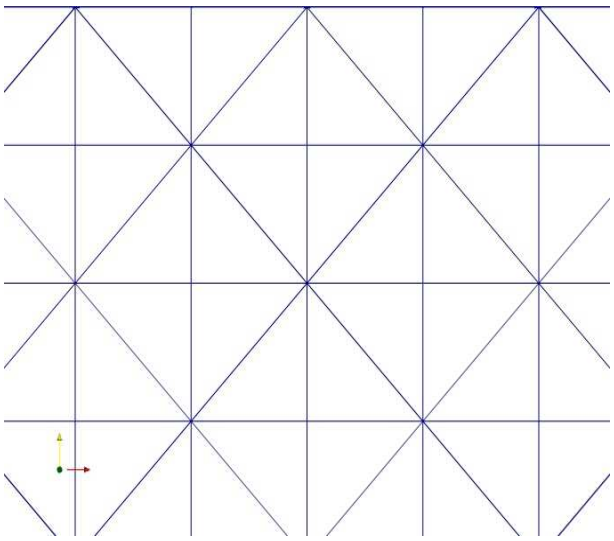

Figure 6: Regular mesh

In the regular case, we plot respectively in FIG. 8 and FIG. 7 the Gaussian translation using the Mass Matrix Central Differencing scheme and the Mass Lumping V6 scheme. One can observe that the translation is well predicted. In the irregular case, as shown FIG. 11, the translation is well predicted with the Mass Matrix Central scheme and using the V6 scheme, one have some perturbations, see FIG. 10.

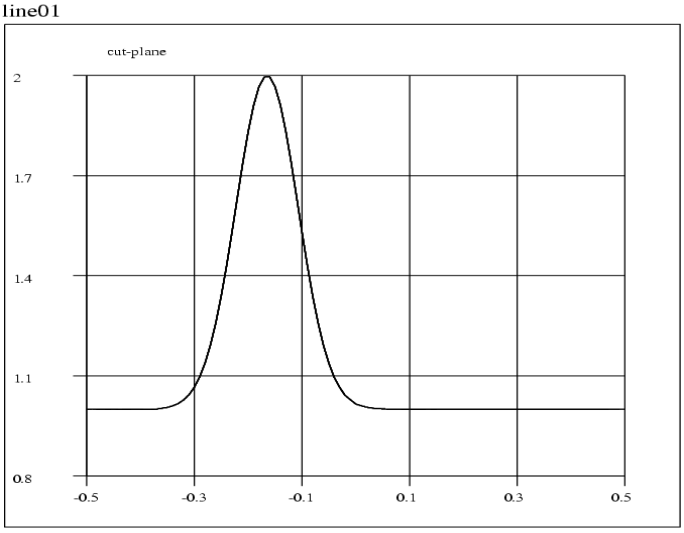

Figure 7: Gaussian translated with the Mass Lumping V6 scheme on regular mesh

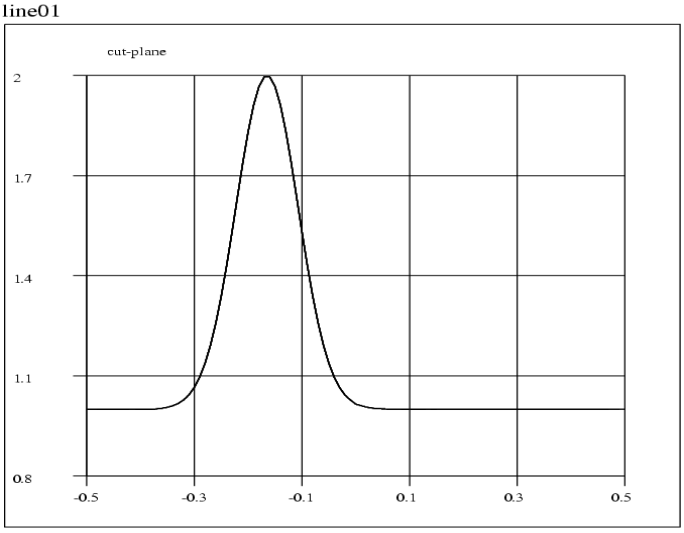

Figure 8: Gaussian translated with the Mass Matrix Central Differencing scheme (with projected dissipation) on regular mesh

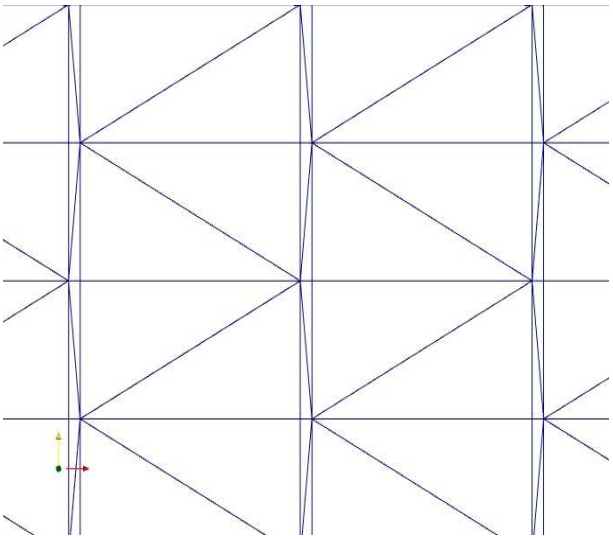

Figure 9: Irregular mesh

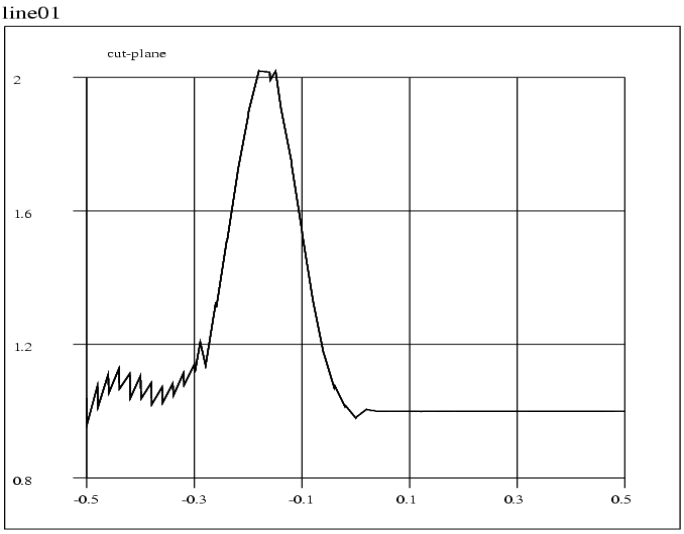

Figure 10: Gaussian translated with the Mass Lumping V6 scheme on irregular mesh

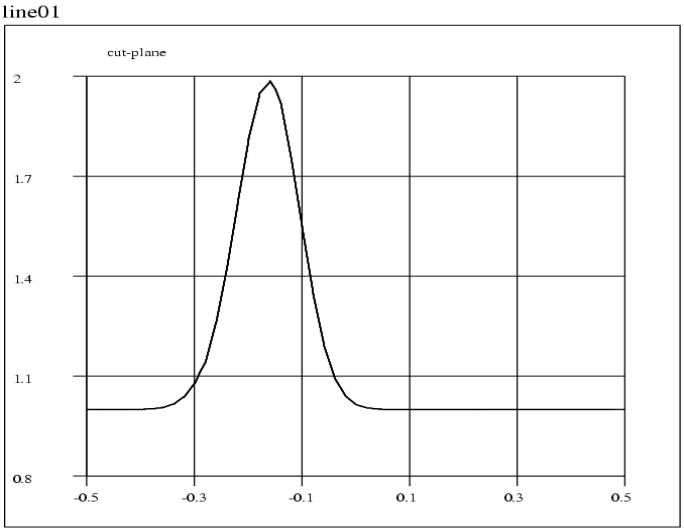

Figure 11: Gaussian translated with the Mass Matrix Central Differencing scheme (with projected dissipation) on irregular mesh

5.2 Applications: Flow around a circular cylinder at Re=3900

VMS-LES is performed to simulate the flow past a circular cylinder at Mach number $M_\infty = 0.1$ and at a subcritical Reynolds number Re_D of 3900 ($\mathrm{Re}_D = \frac{u_\infty D}{\nu}$) based on cylinder diameter D and free-steam velocity u_∞. The computational domain as shown in FIG. 12 is $-10 \leq x/D \leq 25$, $-20 \leq y/D \leq 20$ and $-\pi/2 \leq z/D \leq \pi/2$ where x, y and z denote the streamwise, transverse and spanwise direction respectively. The characteristics of the domain are the following:

$$L_i/D = 10, \quad L_0/D = 25, \quad H_y/D = 20 \quad \text{and} \quad H_z/D = \pi$$

The cylinder of unit diameter is centered on $(x, y) = (0, 0)$.

The flow domain is discretized by an unstructured tetrahedral grid which consists of approximatively 2.9×10^5 nodes. The averaged distance of the nearest point to the cylinder boundary is $0.017D$ which corresponds to $y^+ \approx 3.31$.

For the purpose of these simulations, the Steger-Warming conditions are imposed at the inflow and outflow as well as on the upper and lower surface ($y = \pm H_y$). In the spanwise direction periodic boundary conditions is applied. On the cylinder surface no-slip boundary conditions are set.

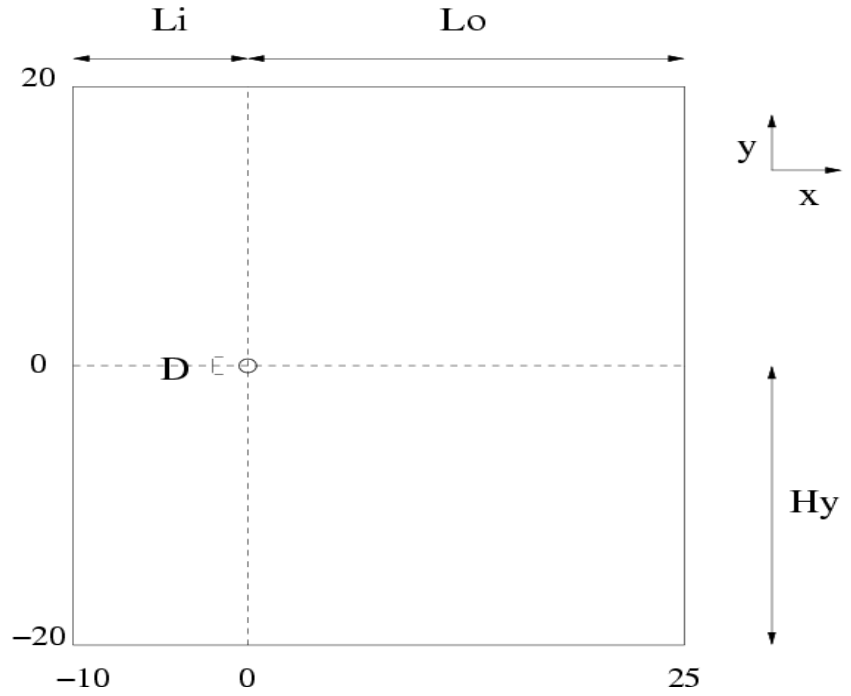

Figure 12: Computational domain

To investigate the influence of numerical schemes on the VMS-LES approach, three simulations have been carried out using the WALE subgrid-scale model. The characteristics of the simulations performed for this study are summarized on TAB. 1. One uses the Roe-Turkel solver as preconditioning. For stability reasons, the mass-matrix scheme has been run setting the numerical viscosity

parameter γ to its maximal value 1. In the same manner, the projected dissipation option is not presented here.

Simulation	Numerical Scheme	Value of constant C	Dissipation	γ	CFL
Simu1	**Mass Matrix + Central Diff.**	$\frac{1}{30}$	**Non projected**	**1**	**20**
Simu2	**Mass Lumping + V6**	$\frac{1}{30}$	**Non projected**	**1**	**20**
Simu3	**Mass Lumping + V6**	$\frac{1}{30}$	**Non projected**	**0.3**	**20**
Simu4	**Mass Matrix + Central differencing**	$\frac{1}{15}$	**Non projected**	**1**	**20**

Table 1: Simulations using VMS-LES approach with the WALE subgrid-scale model, constant C defined in section 3.3 by equation 16

The CFL number has been chosen so that a vortex shedding cycle is sampled in a little less than 1000 time steps. Time-averaged values and turbulence parameters are summarized in TAB. 2 and compared to data from experiments of Norberg , Ong and Wallace and Parnaudeau et al.. $\overline{C_d}$ denotes the mean drag coefficient, $C_d^{'}$ and $C_l^{'}$ respectively the root mean square values of the drag and lift, St the Strouhal number, U_{min} the mean centerline streamwise velocity, Cp_{back} the mean back-pressure coefficient and l_r the mean recirculation length.

	St	$\overline{C_d}$	C_d'	C_l'	U_{min}	Cp_{back}	l_r
Simulations							
Simu1	**0.252**	**0.77**	**0.0157**	**0.0367**	**-0.20**	**-0.66**	**1.76**
Simu2	**0.213**	**1.08**	**0.0490**	**0.4912**	**-0.29**	**-1.09**	**0.83**
Simu3	**0.215**	**1.01**	**0.0639**	**0.5920**	**-0.29**	**-1.02**	**1.08**
Simu4	**0.215**	**1.02**	**0.0103**	**0.0303**	**-0.29**	**-0.94**	**1.12**
Experiments							
[11]	0.215±0.05	0.99±0.05			-0.24±0.1	-0.88±0.05	
[12]	0.21±0.005						1.4 ±0.1
[13]					-0.34		1.51

Table 2: Flow parameters for the present simulations

As shown in TAB. 2, for the same level of numerical dissipation (Simu1, Simu2 and Simu3), the flow parameters obtained with the mass-matrix scheme are generally less well predicted than those obtained with the classical V6 scheme. In particular the mean drag is under-estimated with the mass-matrix scheme, which involves an over-estimation of the recirculation length. Comparing Simu1 and Simu4, one can note that to introduce a numerical dissipation twice bigger significantly improve the results.

FIG. 13 shows a profile of time-averaged and z-averaged streamwise velocity. One can determinize from this plot the most dissipative scheme, that is the scheme producing the most short recirculation length. This assumption is verified on FIG. 14, showing the pressure distribution on the cylinder surface averaged in time on homogeneous z direction. The most dissipative scheme is indeed the one being the most far from the experimental data. From this two plots, one can conclude that the mass-matrix scheme is not enough dissipative. This can explain the encountered robustness problem. Introducing a bigger dissipation level reduce considerably the recirculation length. One can also note FIG. 14 the discrepancies with the experimental data, for θ being be-

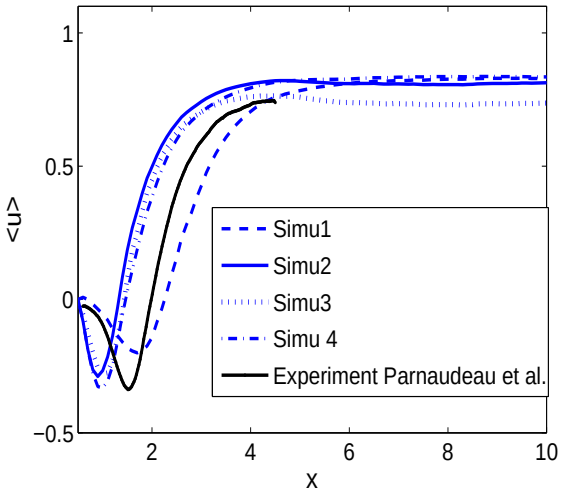

Figure 13: Time-averaged streamwise velocity on the centerline direction

tween 60 and 100. This is probably due to the coarseness of the used grid.

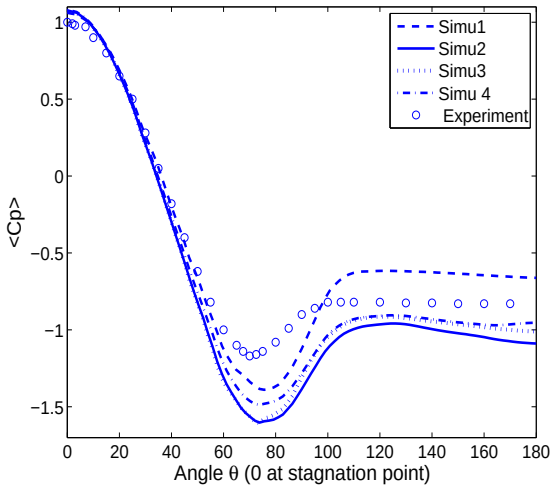

Figure 14: Time-averaged and z-averaged pressure distribution on the surface of the cylinder, experiment: Norberg

FIG. 15 displays the total resolved Reynolds stress $\overline{u'u'}$ in the wake at $x = 1.54$ and FIG. (16) displays the total resolved Reynolds stress $\overline{v'v'}$ at $x = 1.54$. One can observe FIG. 15 that the plot is not symmetric using the mass-matrix scheme. With a low dissipation level, the better results

are obtained with the V6 scheme. The behaviour of the Mass-Matrix scheme is improved using a bigger numerical viscosity.

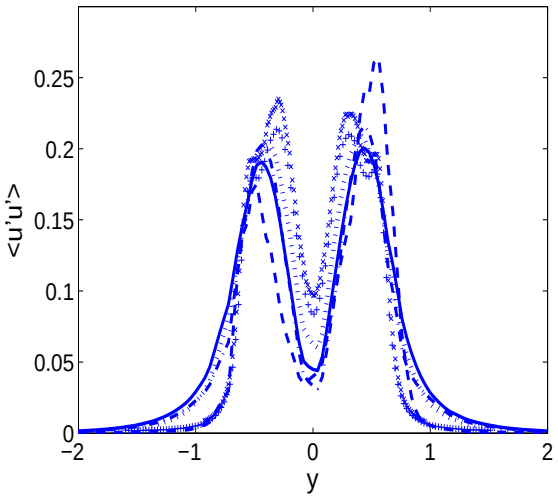

Figure 15: Total resolved streamwise Reynolds stress $< u\prime u\prime >$ at $x = 1.54$, experiments: Parnaudeau et al.; −−: Simu1; −: Simu2;...: Simu3; −.: Simu4; +: PIV1 experiment; ×: PIV2 experiment

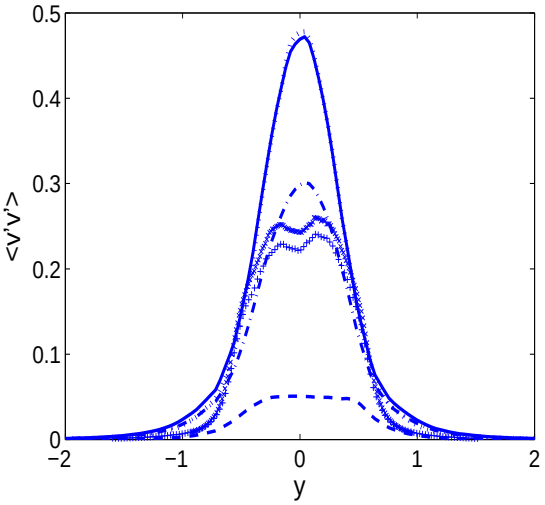

Figure 16: Total resolved streamwise Reynolds stress $< v\prime v\prime >$ at $x = 1.54$, experiments: Parnaudeau et al.;−−: Simu1; −: Simu2;...: Simu3; −.: Simu4; +: PIV1 experiment; ×: PIV2 experiment

In the case of total resolved streamwise Reynolds stress $< v'v' >$ at $x = 1.54$, one can notice first that for the three simulations, we are getting far away from our experiments. The mass lumping V6 scheme still yields better results than the two other ones. But increasing the numerical viscosity for the Mass-Matrix scheme (Simu4) gives a better agreement with the experiments.

6 Conclusion

We have presented in this work a first investigation of a new Mass Matrix scheme, in order to obtain a better accuracy than for Mass Lumping FV scheme on irregular meshes.
This numerics was installed in a parallel code AERO of research and production.
The first results are promising. For the Gaussian translation, the Mass-Matrix clearly improved the prediction using an irregular mesh. We have also shown that the results obtained for the simulation of the flow around a circular cylinder are improved with the Mass-Matrix scheme when a suitable level of numerical dissipation is chosen.
This first work on the Mass-Matrix scheme needs to be continued by investigating the dissipation term and the behavior of this model for the simulation of turbulent flows on strongly irregular three-dimensional meshes.

Acknowlegments: We thank Eric Lamballais for kindly sending us data related to [13]. **CINES** and **INRIA** are gratefully acknowledged for having provided the computational resources.

References

[1] C. Debiez, *Approximation et linéarisation d"ecoulements aérodynamiques instationnaires*, Ph.D Thesis,Université de Nice Sophia-Antipolis,École doctorale-Sciences pour l'ingénieur,(1996).

[2] C. Farhat, A. Kajasekharan and B. Koobus, *A dynamic variational multiscale method for large eddy simulations on unstructured meshes*, Computational Methods in Applied Mechanics and Engineering, (2005), 1668-1691.

[3] J. Hinze, *Turbulence*, MacGraw-Hill, New York, (1959).

[4] T.J.R. Hughes, L. Mazzei and K.E. Jansen. *Large eddy simulation and the variational multiscale method*, Comput. Vis. Sci., 3, (2000), 47-59.

[5] B. Koobus and C. Farhat, *A variational multiscale method for the large eddy simulation of compressible turbulent flows on unstructured meshes-application to vortex shedding*, Comput. Methods Appl. Mech. Eng., 193, (2004), 1367-1383.

[6] B. Koobus, S. Wornom, S. Camarri, M.-V. Salvetti, A. Dervieux *Nonlinear V6 schemes for compressible flow*, Institut National de Recherche en Informatique et Automatique,30 janvier 2008 (2005), 1668-1691.

[7] S. Camarri, M. V. Salvetti, B. Koobus, and A. Dervieux *A low diffusion* MUSCL *scheme for* LES *on unstructured grids*, Comput. Fluids, 33, (2004), 1101–1129.

[8] G.W. Jones, J.J. Cincotta and R.W. Walker, *Aerodynamic forces on a stationary and oscillating circular cylinder at high Reynolds numbers*, National Aeronautics and Space Administration, NASA TR R-300, (1969).

[9] M.H. Lallemand, H. Steve and A. Dervieux. *Unstructured multigridding by volume agglomeration: current status*, Comput. Fluids, 21, (1992), 397-433.

[10] M.H. Lallemand, *Schemas decentres multigrilles pour la resolution des equations d'Euler en elements finis*, Ph.D Thesis,Université de Provence, Centre Saint Charles, (1988).

[11] C. Norberg, *Effects of Reynolds Number and Low-Intensity Free-Sream Turbulence on the Flow around a Circular Cylinder*, Publ. No. 87/2, Department of Applied Termosc. and Fluid Mech., Chalmer University of Technology, Gothenburg, Sweden, (1987).

[12] L. Ong and J. Wallace, *The velocity field of the turbulent very near wake of a circular cylinder*, Exp. in Fluids, vol.20, Springer Verlag Berlin, (1996) ,441-453.

[13] P. Parnaudeau, J. Carlier, D. Heitz and E. Lamballais *Experimentel and numerical studies of the flow over a circular cylinder at Reynolds number 3900*, Phys. of Fluids, 20, (2008).

[14] R. Peyret, *Handbook of computational fluid mechanics*, Academic Press, 2004

[15] P. L. Roe, *Approximate Riemann solvers, parameters, vectors and difference schemes*, J. Comp. Phys., 43, (1981), 357-372.

[16] S. Schmidt and F. Thiele, *Comparison of numerical methods applied to the flow over wall-mounted cubes*, Int. J. of Heat and Fluid Flow, 23, (2002), 330-339.

[17] J. Smagorinsky, *General circulation experiments with the primitive equations*, Monthly Weather Review, 91(3), (1963), 99-164.

[18] J.L. Steger and R.F. Warming, *Flux vector splitting for the inviscid gas dynamic equations with applications to the finite difference methods*, J. Comp. Phys., 40, (1981), 263-293.

[19] B. van Leer, *Towards the ultimate conservative scheme. IV: A new approach to numerical convection*, J. Comp. Phys., 23, (1977), 276-299.

[20] D.C. Wilcox, *Turbulence modeling*, DCW Industries Inc., (1993).

[21] M.M. Zdravkovich, *Flow around circular cylinders*, Oxford University Press, (2003).

Unité de recherche INRIA Sophia Antipolis
2004, route des Lucioles - BP 93 - 06902 Sophia Antipolis Cedex (France)

Unité de recherche INRIA Futurs : Parc Club Orsay Université - ZAC des Vignes
4, rue Jacques Monod - 91893 ORSAY Cedex (France)
Unité de recherche INRIA Lorraine : LORIA, Technopôle de Nancy-Brabois - Campus scientifique
615, rue du Jardin Botanique - BP 101 - 54602 Villers-lès-Nancy Cedex (France)
Unité de recherche INRIA Rennes : IRISA, Campus universitaire de Beaulieu - 35042 Rennes Cedex (France)
Unité de recherche INRIA Rhône-Alpes : 655, avenue de l'Europe - 38334 Montbonnot Saint-Ismier (France)
Unité de recherche INRIA Rocquencourt : Domaine de Voluceau - Rocquencourt - BP 105 - 78153 Le Chesnay Cedex (France)

Éditeur
INRIA - Domaine de Voluceau - Rocquencourt, BP 105 - 78153 Le Chesnay Cedex (France)
http://www.inria.fr
ISSN 0249-6399